femington

Int. J. Clin. Res. Med. Sci. (2026) 1(3):1–18
Article ID: IJCRMS-2026-678

Optimized Intensity Modulated Radiation Therapy: A Multi-Objective Approach for Balancing Tumor Control and Organ Preservation

Parulben Patel
drparulpatel@gmail.com
Independent Researcher

Abstract

Intensity-Modulated Radiation Therapy (IMRT) is a highly precise cancer treatment method that utilizes beamlets to deliver targeted radiation doses, aiming to maximize tumor eradication while minimizing damage to surrounding healthy tissues. This study presents an optimization framework for IMRT treatment planning, incorporating a mixed-integer programming model to address dose distribution challenges. We propose three distinct treatment strategies, each obtained by solving a separate Multi-objective mixed-integer program under a different objective and/or set of enforced constraints. The three plans are intended to illustrate alternative trade-offs between tumor coverage and healthy-tissue sparing, rather than to constitute points on a formally derived Pareto front. The formulation employs two alternative single-objective functions: one maximizing the total CTV dose and the other minimizing the total non-CTV dose. The results demonstrate the behavior of the model under these alternative formulations, providing illustrative trade-offs for decision-making; however, no formal multi-objective scalarization or Pareto-based procedure is presented.

Keywords

• Intensity Modulated Radiation Therapy (IMRT) • Mixed-Integer Programming (MIP) • Multi-Objective Optimization • Dose-Volume Constraints • Radiation Treatment Planning

1. Introduction

Intensity Modulated Radiation Therapy (IMRT) is an effective approach in cancer treatment. The main idea is to utilize beamlets to irradiate patients to kill tumor cells, while protecting healthy organs as much as possible. Therefore, the treatment plan can be formulated as an optimization problem. Recent advances in computational optimization have enabled increasingly sophisticated approaches to treatment planning, including mixed-integer linear programming formulations for beam angle optimization [1] and deep reinforcement learning strategies for beam angle selection [2]. These developments reflect a broader trend toward automating and optimizing radiotherapy planning processes.

In this project, we propose three radiation treatment plans, each obtained by solving a separate single-objective mixed-integer program under a different objective and/or set of enforced constraints. These plans are intended to illustrate alternative trade-offs between safety and efficacy, rather than to constitute solutions to a formally defined multi-objective optimization problem. No Pareto-based or scalarized multi-objective procedure was employed. Different patients may have distinct preferences regarding safety and efficacy; the plans presented here are illustrative of how the optimization framework behaves under alternative single-objective formulations, and are not clinical recommendations.

© 2026 Femington Academic Publishing. All rights reserved.

We emphasize that the results presented in this manuscript are derived from a mathematical optimization model evaluated on a single computational test case, and do not constitute a clinically validated treatment-planning outcome. The evaluation is based on a single 2D computational geometry with 400 voxels and 60 beamlets; no additional test cases, patient geometries, or 3D anatomical datasets were used. Any statements regarding patient-specific treatment selection, effectiveness, or clinical benefit should be interpreted as illustrative of the optimization framework's behavior on this single test case rather than as clinical recommendations or evidence of robustness. Validation across multiple patients and geometries remains future work.

2. Related Work

The application of optimization techniques to radiotherapy treatment planning has a rich history spanning several decades. Early work focused on inverse planning methods, while more recent efforts have leveraged advanced computational techniques to address increasingly complex planning problems. In this section, we review relevant literature across several key areas: beam angle optimization, mixed-integer programming approaches, machine learning applications, and multi-objective optimization frameworks.

2.1 Beam Angle Optimization

Beam angle optimization (BAO) remains a challenging combinatorial problem in radiotherapy planning. Huang et al. [1] applied mixed-integer linear programming to the non-coplanar beam angle optimization problem for liver cancer IMRT, demonstrating that MILP can effectively handle the discrete nature of beam angle selection while optimizing dose distribution. Their approach highlights the computational tractability of exact optimization methods for clinically relevant problem sizes. In a complementary direction, Bao et al. [2] developed a deep reinforcement learning framework for beam angle optimization, treating the sequential selection of beam angles as a Markov decision process. This learning-based approach offers potential advantages in computational efficiency compared to exact methods, particularly for larger problem instances.

2.2 Mixed-Integer Programming in Radiotherapy

Mixed-integer programming has been successfully applied to various radiotherapy optimization problems beyond beam angle selection. Shinde et al. [3] formulated a mixed-integer programming approach to minibeam aperture optimization for multi-collimator proton minibeam radiotherapy, addressing the unique challenges posed by proton therapy. Their work demonstrates the versatility of MIP formulations in handling different treatment modalities and planning objectives. The present study builds upon this tradition by formulating a mixed-integer program for IMRT treatment planning that incorporates binary decision variables to handle dose-volume constraints, similar to the approaches reviewed above. Pre-trained mixed-integer optimization techniques [4] provide additional methodological tools that can inform such formulations. Robust and fractional optimization models have also been developed for related sparse and multiobjective settings [5, 6].

2.3 Machine Learning and Automation in Treatment Planning

The integration of machine learning and artificial intelligence into radiotherapy planning has gained significant momentum in recent years. Wu et al. [7] developed an automated treatment planning system for pancreatic SBRT using reinforcement learning, demonstrating that RL agents can learn to generate

clinically acceptable plans. Jiang et al. [8] provided an overview of AI-driven radiotherapy optimization, emphasizing the integration of machine learning with inverse planning methods. These studies illustrate the potential for learning-based approaches to augment or replace traditional optimization pipelines in specific clinical scenarios.

2.4 Multi-Objective Optimization and Pareto Methods

Multi-objective optimization is particularly relevant to radiotherapy planning, where trade-offs between tumor coverage and organ-at-risk sparing are inherent. Craft et al. [9] addressed the challenge of approximating convex Pareto surfaces in multiobjective radiotherapy planning, providing methods for navigating the trade-off space between competing objectives. Earlier work by Craft et al. [10] established foundational methods for approximating convex Pareto surfaces in multiobjective radiotherapy planning. The normal-boundary intersection method of Das and Dennis [11] provides a general approach for generating Pareto surfaces in nonlinear multicriteria optimization problems. Test instance generators for multiobjective mixed-integer optimization [12] further support systematic benchmarking of such methods. Their work establishes a formal framework for understanding the Pareto frontier in treatment planning, which contrasts with the illustrative single-objective approach adopted in the present study.

2.5 Normal Tissue Tolerance and Dose Constraints

The dose constraints employed in radiotherapy planning are grounded in extensive clinical research on normal tissue tolerance. Emami et al. [13] provided foundational tolerance data for normal tissues exposed to therapeutic irradiation, establishing dose-volume relationships that continue to inform modern planning constraints. Marks et al. [14] reviewed the use of normal tissue complication probability models in clinical practice, offering guidance on translating tolerance data into practical planning objectives. For specific organs, Michalski et al. [15] summarized radiation dose-volume effects in the rectum, while Daoud et al. [16] examined avascular necrosis of the femoral head following palliative radiotherapy, highlighting the dose-dependent risks to bone structures.

2.6 Clinical Guidelines and Reporting Standards

Clinical practice guidelines and reporting standards provide essential context for radiotherapy planning. The National Comprehensive Cancer Network [17] publishes regularly updated guidelines for prostate cancer treatment, including recommendations for definitive radiotherapy. The International Commission on Radiation Units and Measurements [18] established standards for prescribing, recording, and reporting photon-beam IMRT, including recommendations for dose homogeneity within target volumes. These standards are complemented by methodological work on robust optimization for treatment planning under uncertainty [5].

2.7 Emerging Applications of Computational Methods in Medicine

Beyond radiotherapy planning, computational and data-driven methods are increasingly applied across medical domains. Rajendran [19] developed personalized prediction models for lymph node involvement in head and neck squamous cell carcinomas using mixture hidden Markov models. These works illustrate the broader ecosystem of computational methods applied in medical research.

3. Analysis

3.1 Classification

Voxels on the boundaries of organs are sometimes misclassified due to the variability of the positions of patients. If tumor cells are not getting enough radiation, they might be able to grow again. To make up variations, voxels on the edge of the CTV region are classified as CTV if possible. We propose the voxel classifications in Figure 1.

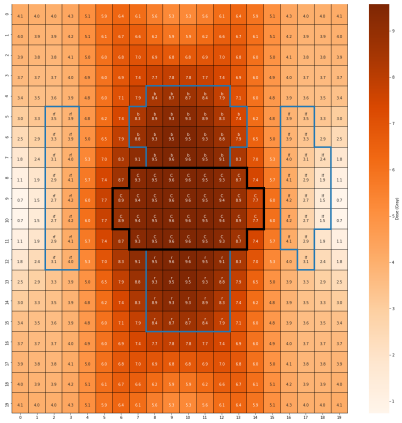


Figure 1: Classification of Voxels

Figure 1 shows the classifications of 400 voxels and their doses when all beamlets have exactly one intensity. The voxels in the black bounding box with letter C are considered as the CTV region. The voxels in the blue bounding boxes are Bladder (b), Rectal Solid (r), Left Femur Head (lf), and Right Femur Head (rf), respectively. Other voxels are classified as Unspecified. The color of each voxel reflects the dose received.

The anatomical and treatment context represented by this computational test case is a simplified 2D axial cross-section of the male pelvis, representative of a prostate cancer treatment scenario. The CTV corresponds to the prostate gland, and the bladder, rectum, and femoral heads are the primary organs at risk. The prescription dose of 80 Gy in 40 fractions is representative of definitive intensity-modulated radiation therapy for localized prostate cancer [17]. This simplified geometry is intended for proof-of-concept evaluation of the optimization framework and does not capture full 3D anatomy, organ motion, or patient-specific variability.

With classifications of each voxel, we are able to formulate this optimization as a mixed linear and integer programming problem.

3.2 Formulation

Before formulation, we declare some of the notations that will be mentioned later. For example, in the Bladder region:

- $\{Bladder\}$ denotes the voxels that belong to the Bladder region.

- $|Bladder|$ denotes the number of voxels in the Bladder region.

3.2.1 Decision Variables

Beamlet Intensity
Intuitively, the intensities of beamlets determine the radiation doses received by all voxels.

$$x_i = \text{the intensity of beamlet i}, \quad \forall i \in \{1, 2, \ldots 60\}$$

Besides, some regions have special constraints. For example, at most 10% of the bladder should receive a dose > 65.0 Gy. Those constraints introduce non-linearity and require to use binary decision variables. Therefore, we also incorporate the following decision variables in Bladder, Left Femur Head and Right Femur Head:

Bladder

$$b_j = \begin{cases} 0, & \text{if} \quad D_j > 65.0 \\ 1, & D_j \leq 65.0 \end{cases} \quad \forall j \in \{\text{Bladder}\}$$
$$o_j = \text{the difference between the actual dose and 65.0 Gy} \quad \forall j \in \{\text{Bladder}\}$$

Where:

- b_j denotes if the voxel has a dose no more than 65.0 Gy. if b_j is 1, then the dose is less than or equal 65 Gy.
- o_j denotes the difference between the actual dose D_j and 65.0 Gy. In other words, o_j is the "overdose" or "underdose" compared to 65.0 Gy.
- D_j denotes the radiation received by voxel j. Mathematically, $o_j = D_j - 65$.

Similarly, we have decision variables for left femur head and right femur head:

Left Femur Head

$$b_j = \begin{cases} 0, & \text{if} \quad D_j > 40.0 \\ 1, & D_j \leq 40.0 \end{cases} \quad \forall j \in \{\text{Left Femur}\}$$
$$o_j = \text{the difference between the actual dose and 40.0 Gy} \quad \forall j \in \{\text{Left Femur}\}$$

Right Femur Head

$$b_j = \begin{cases} 0, & \text{if} \quad D_j > 40.0 \\ 1, & D_j \leq 40.0 \end{cases} \quad \forall j \in \{\text{Right Femur}\}$$
$$o_j = \text{the difference between the actual dose and 40.0 Gy} \quad \forall j \in \{\text{Right Femur}\}$$

3.2.2 Objective

The overall goal is to satisfy the constraints as much as possible. In the formulation, we define two alternative single-objective functions, each used separately in a distinct optimization run:

- Maximize the total dose in the CTV region, while satisfying constraints:

$$\max \sum_{j\in\{\text{CTV}\}} \sum_{i=1}^{60} x_i w_{i,j}$$

where $w_{i,j}$ denotes the dose received by voxel j from beamlet i with unit intensity. For simplicity, we denote $D_j = \sum_{i=1}^{60} x_i w_{i,j}$ to be the dose received by voxel j.

- Minimize the total dose received in healthy regions (non-CTV region), while satisfying constraints:

$$\min \sum_{j\notin\{\text{CTV}\}} \sum_{i=1}^{60} x_i w_{i,j}$$

These two single-objective functions reflect alternative priorities between efficacy and safety. The first is more "aggressive" in that it aims to give high radiation doses to tumor cells. The second is more "conservative" as it tries to protect healthy cells as much as possible. Each plan reported in Section 3 is obtained by solving one of these single-objective problems under a specified set of enforced constraints; no weighted sum, epsilon-constraint, or Pareto-based multi-objective method was used.

3.2.3 Constraints

Although not all constraints in the prompt can be satisfied, we will list the constraints mentioned in the prompt and show the variations of them in each specific plan.

CTV

For this computational test case, the CTV dose bounds below are illustrative parameter choices used to demonstrate the optimization framework. The values are not derived from a cited clinical tolerance and should not be interpreted as a patient-specific clinical prescription.

$$80.8 \le D_j \le 84.8 \quad \forall j \in \{\text{CTV}\} \tag{1}$$

Bladder

$$\sum_{j\in\{\text{Bladder}\}} D_j \le |Bladder| \times 50.0 \tag{2}$$

$$o_j = D_j - 65.0 \quad \forall j \in \{\text{Bladder}\} \tag{3}$$

$$o_j \le (81 - 65)(1 - b_j) \quad \forall j \in \{\text{Bladder}\} \tag{4}$$

$$o_j \ge -65 b_j \quad \forall j \in \{\text{Bladder}\} \tag{5}$$

$$\sum_{j\in\{\text{Bladder}\}} b_j \ge 90\% \times |Bladder| \tag{6}$$

Rectum

$$D_j \le 79.2 \quad \forall j \in \{\text{Rectum}\} \tag{7}$$

$$\sum_{j\in\{\text{Rectum}\}} D_j \le |Rectum| \times 40.0 \tag{8}$$

Unspecified

For this computational test case, the 72.0 Gy unspecified-region limit is an illustrative parameter choice used to demonstrate the optimization framework. It is not derived from a cited clinical tolerance and should not be interpreted as a clinically validated dose limit.

$$D_j \le 72.0 \quad \forall j \in \{\text{Unspecified}\} \tag{9}$$

Left Femur Head

$$o_j = D_j - 40.0 \quad \forall j \in \{\text{Left Femur}\} \tag{10}$$

$$o_j \leq (50 - 40)(1 - b_j) \quad \forall j \in \{\text{Left Femur}\} \tag{11}$$

$$o_j \geq -40 b_j \quad \forall j \in \{\text{Left Femur}\} \tag{12}$$

$$\sum_{j \in \{\text{Left Femur}\}} b_j \geq 85\% \times |LeftFemur| \tag{13}$$

Right Femur Head

$$o_j = D_j - 40.0 \quad \forall j \in \{\text{Right Femur}\} \tag{14}$$

$$o_j \leq (50 - 40)(1 - b_j) \quad \forall j \in \{\text{Right Femur}\} \tag{15}$$

$$o_j \geq -40 b_j \quad \forall j \in \{\text{Right Femur}\} \tag{16}$$

$$\sum_{j \in \{\text{Right Femur}\}} b_j \geq 85\% \times |RightFemur| \tag{17}$$

Where,

- (1) denotes the lower limit and the upper limit of dose in the CTV region. For this test case, 80.8 Gy and 84.8 Gy are arbitrary test-case values chosen to illustrate the optimization framework, not a patient-specific clinical prescription. They are intended to avoid "cold spots" and "dose hotspots" and to keep the CTV doses within 5% of each other. The prescription dose of 80 Gy is representative of definitive radiotherapy for localized prostate cancer, and the ICRU-83 recommendation that the prescribed dose to the planning target volume should remain within −5% to +7% of the prescription dose [18] motivates the general order of these bounds, but the specific values 80.8–84.8 Gy are arbitrary test-case choices.

- (2) denotes the average dose of Bladder voxels should be no more than 50.0 Gy. (3), (4), (5), and (6) denote at most 10% of Bladder should receive a dose > 65.0 Gy and the dose should be within range 0 - 81 Gy. These thresholds are based on the QUANTEC bladder dose–volume recommendations, which suggest keeping the bladder volume receiving > 65 Gy below 10–15% to limit the risk of grade ≥ 2 genitourinary toxicity [14]. The average bladder dose constraint of 50 Gy is consistent with institutional protocols for prostate IMRT. To interpret this:

  - The left hand side of (6) denotes the total number of voxels in Bladder that are ≤ 65.0 Gy. The right hand side of (6) means the total number of voxels in Bladder. This means no less than 90% of the Bladder should receive ≤ 65.0 Gy.
  - (3) denotes o_j is the difference between the actual dose and 65.0 Gy.
  - (4) and (5) denote the relationship between o_j and b_j. When $b_j = 0$, $0 \leq o_j \leq 16$, which means the maximum dose should not exceed 81.0 Gy. When $b_j = 1$, $-65 \leq o_j \leq 0$, which means the minimum dose should not be less than 0.

- (7) and (8) denote that in the Rectum, maximum dose should be ≤ 79.2 Gy, and the average dose should be ≤ 40.0 Gy. These limits are based on the QUANTEC rectum dose–volume recommendations, which indicate that keeping the rectal maximum dose below approximately 75–80 Gy and the mean dose below 40 Gy reduces the risk of grade ≥ 2 gastrointestinal toxicity [15]. The specific value of 79.2 Gy corresponds to 99% of the 80 Gy prescription dose.

- (9) denotes the maximum dose in the Unspecified region should be ≤ 72.0 Gy. For this test case, the specific 72.0 Gy value is an arbitrary test-case value used to illustrate the optimization framework and is not derived from a cited clinical tolerance. This constraint is a planning heuristic intended to limit dose to unspecified soft tissue and avoid unintended hotspots outside the explicitly contoured organs. The value of 72 Gy corresponds to 90% of the 80 Gy prescription dose and is consistent with the general intent of ICRU recommendations for dose homogeneity outside target volumes, but the specific value is arbitrary for this test case.

- (10), (11), (12) and (13) denote the maximum dose of Left Femur Head should be ≤ 50.0 Gy, and no more than 15 % of them should be ≥ 40.0 Gy. These constraints are based on the well-documented dose-dependent risk of radiation-induced avascular necrosis (osteonecrosis) of the femoral head [13, 16]. The QUANTEC femoral head recommendations suggest keeping the maximum dose below 50 Gy and limiting the volume receiving ≥ 40 Gy to reduce the risk of osteonecrosis.

- (14), (15), (16) and (17) denote the maximum dose of Right Femur Head should be ≤ 50.0 Gy, and no more than 15 % of them should be ≥ 40.0 Gy. The same clinical rationale as for the Left Femur Head applies.

3.3 Approach

If all constraints above are used, the solver can not find a feasible solution. Therefore, we try to rank constraints in terms of their importance. The idea is to start from the most important constraint, add one constraint at a time until there is no feasible solution. Then, we can slack some constraints. Here are some assumptions we make when solving the optimization problem:

1. If the radiation of CTV is too low, then tumor cells may stay alive and grow back again. Therefore, having enough doses in the CTV region is the priority.

2. The femoral heads are treated as high-priority organs at risk because of the well-documented, dose-dependent risk of radiation-induced avascular necrosis (osteonecrosis) of the femoral head [13, 16]. We therefore do not slack constraints on the Left Femur Head or Right Femur Head unless we have to.

3. Bladder and Rectum are close to the CTV region. It's unavoidable that they receive higher doses than other regions. Lowering the peak dose has the priority than limiting the average dose in the region.

Because the full constraint set defined in Section 3.2.3 is infeasible for this test case, each of the three plans reported in Section 3 is obtained by solving a separate single-objective mixed-integer program under a different objective (maximizing CTV dose or minimizing non-CTV dose) and/or a different set of enforced (relaxed) constraints. No formal multi-objective scalarization or Pareto-based procedure was used to generate these plans. To avoid ambiguity, Tables 1–3 report three quantities for each dosimetric criterion:

- **Actual Dose**: the dose value actually achieved by the optimized plan.

- **Ideal Constraint (Original, Unrelaxed)**: the original bound stated in Section 3.2.3, prior to any relaxation.

Where the Constraint (Enforced) column differs from the Ideal Constraint (Original, Unrelaxed) column, this reflects an explicit, intentional constraint relaxation made under the priority rules above, and not an inconsistency between the reported results and the formulation in Section 3.2.3. The tables use the following conventions:

- CTV Avg is reported for descriptive purposes only. It was not an enforced constraint, and the original formulation in Section 3.2.3 did not impose a CTV average-dose bound; therefore, both the Constraint (Enforced) and Ideal Constraint (Original, Unrelaxed) entries for CTV Avg are shown as "–".
- CTV Per denotes the CTV dose variation implied by the enforced CTV minimum and maximum bounds. The original CTV bounds imply an ideal variation of 5%; the enforced variations under the midpoint definition are 4.83%, 8.25%, and 7.25% in Plans A–C, respectively.
- In Plan A, the achieved CTV Per is computed from the actual achieved doses (CTV Max = 84.8 Gy, CTV Min = 80.8 Gy, CTV Avg = 82.6 Gy), yielding $(84.8 - 80.8)/82.6 \times 100\% = 4.84\%$. The enforced CTV Per is computed from the enforced bounds (84.8 Gy and 80.8 Gy) relative to the midpoint of those bounds, 82.8 Gy, yielding $(84.8 - 80.8)/82.8 \times 100\% = 4.83\%$. The table reports both the actual achieved variation and the enforced variation for transparency. The nominal 5% value originally stated for Plan A was not the result of the stated midpoint calculation; the midpoint calculation gives 4.83%.
- In Plan B, the achieved CTV Per is computed from the actual achieved doses (CTV Max = 85.8 Gy, CTV Min = 79 Gy, CTV Avg = 82.11 Gy), yielding $(85.8 - 79)/82.11 \times 100\% = 8.28\%$. The enforced CTV Per is computed from the enforced bounds (85.8 Gy and 79 Gy) relative to the midpoint of those bounds, 82.4 Gy, yielding $(85.8 - 79)/82.4 \times 100\% = 8.25\%$. The table reports both the actual achieved variation and the enforced variation for transparency.
- In Plan C, the achieved CTV Per is computed from the actual achieved doses (CTV Max = 85.8 Gy, CTV Min = 79.8 Gy, CTV Avg = 82.12 Gy), yielding $(85.8 - 79.8)/82.12 \times 100\% = 7.31\%$. The enforced CTV Per is computed from the enforced bounds (85.8 Gy and 79.8 Gy) relative to the midpoint of those bounds, 82.8 Gy, yielding $(85.8 - 79.8)/82.8 \times 100\% = 7.25\%$. The table reports both the actual achieved variation and the enforced variation for transparency.
- Bladder Per (> 65 Gy) is the fraction of Bladder voxels receiving more than 65 Gy. The original (unrelaxed) limit is 10%; the enforced limits are 25%, 20.83%, and 25% in Plans A–C, respectively.
- The Bladder Avg bound is relaxed from the original 50.0 Gy to 60.0 Gy in Plans A and B and to 57.0 Gy in Plan C, as reported in Tables 1–3.
- The Rectum Avg bound is relaxed from the original 40.0 Gy to 55.0 Gy in Plan A, 45.0 Gy in Plan B, and 55.0 Gy in Plan C.
- The Unspecified Max bound is relaxed from the original 72.0 Gy to 82.0 Gy in Plan A, 83.0 Gy in Plan B, and 77.0 Gy in Plan C.
- In Plan B, the Left and Right Femur Head Max bounds are reported as 50.0 Gy in Table 2, matching the original (unrelaxed) limits. This reflects the final solver configuration used for the reported solution; the actual achieved doses (48.86 Gy and 47.30 Gy for Left and Right Femur Head, respectively) are both below the 50.0 Gy limit.

- The enforced bounds reported in Tables 1–3 for Bladder Avg, Rectum Avg, Bladder Per (> 65 Gy), and Unspecified Max are the bounds used in the mixed-integer program for each plan, as recorded in the solver configuration for the reported solutions. The original (unrelaxed) limits are exceeded in all three plans; these deviations are deliberate constraint relaxations made to obtain feasible solutions. The enforced bounds are: Bladder Avg at 60.0 Gy in Plans A and B and at 57.0 Gy in Plan C; Rectum Avg at 55.0 Gy in Plan A, 45.0 Gy in Plan B, and 55.0 Gy in Plan C; Bladder Per (> 65 Gy) at 25% in Plan A, 20.83% in Plan B, and 25% in Plan C; and Unspecified Max at 82.0 Gy in Plan A, 83.0 Gy in Plan B, and 77.0 Gy in Plan C. The actual achieved doses are all within the enforced bounds, consistent with the enforced constraints.

In particular, Plans B and C report CTV minimum and maximum doses outside the original arbitrary test-case 80.8–84.8 Gy range. These deviations are deliberate constraint relaxations: for Plan B, the CTV minimum is relaxed from 80.8 Gy to 79 Gy and the CTV maximum from 84.8 Gy to 85.8 Gy; for Plan C, the CTV minimum is relaxed from 80.8 Gy to 79.8 Gy and the CTV maximum from 84.8 Gy to 85.8 Gy. The rationale is that the original arbitrary test-case CTV bounds, together with the other organ-at-risk constraints, rendered the full constraint set infeasible. Relaxing the CTV bounds allows the solver to find feasible solutions that still maintain clinically desirable CTV coverage while satisfying the remaining constraints as closely as possible. The optimization consequence is a slightly wider CTV dose range (up to 8.28% and 7.31% variation in Plans B and C, respectively, versus 4.84% in Plan A), which reflects the trade-off between strict CTV uniformity and feasibility under the full constraint set.

4. Results

With OR-Tools, we solve each single-objective mixed-integer program separately. Here we present three treatment plans, each obtained under a different objective and/or set of enforced constraints. These plans are illustrative of alternative trade-offs and do not constitute a formally derived Pareto front.

4.1 Plan A

The Plan A is the most “effective” yet “aggressive” plan as it satisfies constraints in the CTV region and Femur Heads, while risking other healthy organs. The objective is to maximizing the total doses received in the CTV region. That is:

$$\max \sum_{j \in \{\mathrm{CTV}\}} D_j$$

The following table shows the constraints set for this plan and the actual dose received by each region.

Table 1: Doses and Constraints of Plan A

	Actual Dose	**Constraint (Enforced)**	**Ideal Constraint (Original)**
CTV Max	84.8	84.8	84.8
CTV Min	80.8	80.8	80.8
CTV Avg	82.6	–	–
CTV Per	4.84%	4.83%	5%
Bladder Max	74.67	81	81
Bladder Avg	58.89	60	50
Bladder Per (> 65)	25.00%	25%	10%
Rectum Max	76.19	79.2	79.2
Rectum Avg	55	55	40
Unspecified Max	82	82	72
Left Femur Max	47.65	50	50
Left Femur Per (> 40)	10.53%	15%	15%
Right Femur Max	47.30	50	50
Right Femur Per (> 40)	12.50%	15%	15%

4.1.1 Dose Distribution of A

Figure 2 shows the dose distribution of Plan A. As we can see from the figure, both femur heads are well protected from the radiation. To compensating variations of positions of patients, voxels on the boundary of the CTV region are also highly radiated. This allows the radiation to kill tumor cells in multiple days. However, Bladder and Rectum cells that are close to the CTV region might be vulnerable.

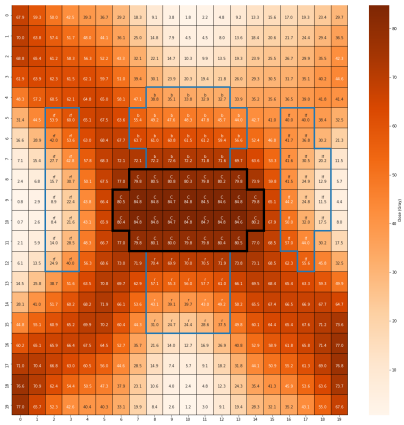


Figure 2: Dose Distribution of Plan A

4.1.2 Beamlet Intensity of A

The following figure shows intensities of all beamlets from 1 to 60. To interpret this, each row of the plot means the 6 different angles of the beam, and the columns are the 10 beamlets in each angle. The solution is relatively sparse as some beamlets have high intensities while other are basically unused. This implies under this setting of constraints, some beamlets have much higher priority than others. Similar sparsity patterns have been observed in other optimization-based treatment planning studies [6].

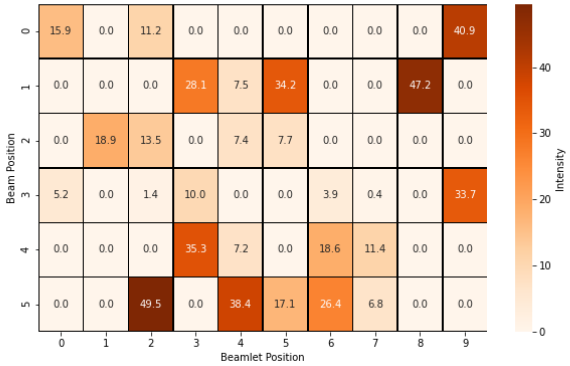


Figure 3: Beamlet Intensity of Plan A

4.2 Plan B

Compared to the Plan A, Plan B is less "aggressive" on the Bladder and Rectum, especially on the voxels that are connected to the CTV region. However, Plan B has higher radiation variance on the CTV region, and the Unspecified region may have a "dose hotspot". Similarly to Plan A, both Femur Heads are well protected as they are sensitive to the radiation. The objective is set to be minimizing the total doses received by all healthy regions (voxels that are not in the CTV region). That is:

$$\min \sum_{j \notin \{\text{CTV}\}} D_j$$

The following table shows the constraints set for this plan and the actual dose received by each region. Robust optimization formulations provide one avenue for managing the uncertainty reflected in these trade-offs [5].

Table 2: Doses and Constraints of Plan B

	Actual Dose	**Constraint (Enforced)**	**Ideal Constraint (Original)**
CTV Max	85.8	85.8	84.8
CTV Min	79	79	80.8
CTV Avg	82.11	–	–
CTV Per	8.28%	8.25%	5%
Bladder Max	75.51	81	81
Bladder Avg	56.02	60	50
Bladder Per (> 65)	20.83%	20.83%	10%
Rectum Max	71.15	79.2	79.2
Rectum Avg	45	45	40
Unspecified Max	83	83	72
Left Femur Max	48.86	50	50
Left Femur Per (> 40)	10.53%	15%	15%
Right Femur Max	47.30	50	50
Right Femur Per (> 40)	12.50%	15%	15%

4.2.1 Dose Distribution of B

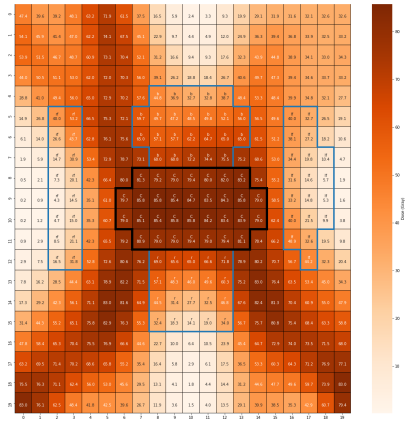


Figure 4: Dose Distribution of Plan B

4.2.2 Beamlet Intensity of B

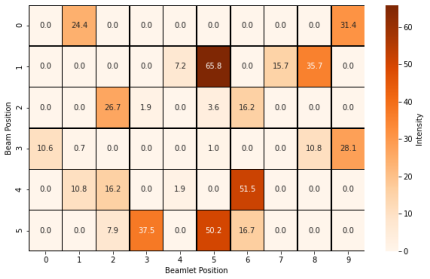


Figure 5: Beamlet Intensity of Plan B

4.3 Plan C

In order to avoid a "dose hotspot" in the Unspecified region, we propose Plan C. Plan C delivers higher doses in the CTV region and Femur Heads but decreases the peak dose in the Unspecified region. Similar to Plan B, The objective is to set to be minimizing the total doses received by all healthy regions. Pre-trained mixed-integer optimization techniques may help improve solver performance for such formulations [4].

$$\min \sum_{j \notin \{\text{CTV}\}} D_j$$

The following table shows the constraints set for this plan and the actual dose received by each region.

Table 3: Doses and Constraints of Plan C

	Actual Dose	**Constraint (Enforced)**	**Ideal Constraint (Original)**
CTV Max	85.8	85.8	84.8
CTV Min	79.8	79.8	80.8
CTV Avg	82.12	–	–
CTV Per	7.31%	7.25%	5%
Bladder Max	74.42	81	81
Bladder Avg	57.00	57	50
Bladder Per (> 65)	25.00%	25.00%	10%
Rectum Max	72.44	79.2	79.2
Rectum Avg	54.68	55	40
Unspecified Max	77	77	72
Left Femur Max	49.09	50	50
Left Femur Per (> 40)	10.53%	15%	15%
Right Femur Max	44.54	50	50
Right Femur Per (> 40)	12.50%	15%	15%

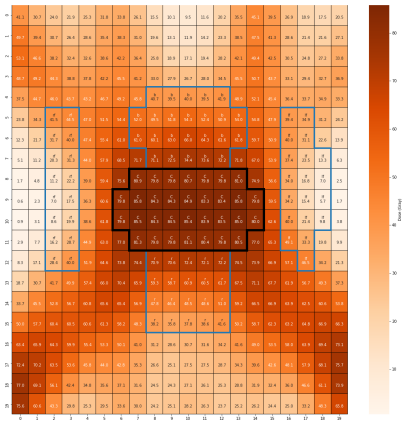


Figure 6: Dose Distribution of Plan C

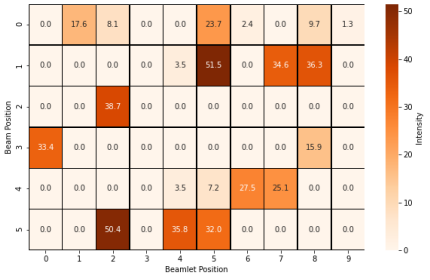


Figure 7: Beamlet Intensity of Plan C

5. Conclusion

We summarize 3 treatment plans we proposed. Every plan has pros and cons, so each plan may be targeted to a certain type of patients. Based on the optimization problems we solved, we can get a sense of how plans should be delivered. The normal-boundary intersection method provides a general strategy for generating Pareto surfaces in multicriteria optimization [11], while earlier work on approximating convex Pareto surfaces in radiotherapy planning offers additional context for interpreting trade-offs [10].

Table 4: Summary of 3 Plans

Name	Pros	Cons	Target Patients
Plan A	• Uniform radiation in CTV without "cold spot" • Femur Heads are well protected • Edges are highly radiated	• High radiation in Bladder and Rectum on average	• Patients who seek the most effective plan
Plan B	• Lower radiation in Bladder and Rectum on average • Femur Heads are well protected	• Some "cold spots" on the edge of CTV • Peak radiation in the Unspecified region	• Patients who have sensitive Bladder or Rectum cells
Plan C	• Relatively uniform dose in CTV • Low peak in the Unspecified region • Femur Heads are well protected	• Relatively high radiation in Bladder and Rectum	• Patients who have sensitive cells in the Unspecified region

Note: The "Target Patients" descriptors above are qualitative characterizations of each plan's dosimetric trade-offs on the single computational test case studied here. They are not clinical treatment-selection recommendations and have not been validated against clinical outcomes data. Similar caution regarding clinical translation has been emphasized in prior automated planning work [7].

6. Discussion

6.1 Trade-off

Based on the three single-objective plans we have, binding constraints are often among the "Minimum CTV Dose", "Maximum CTV Dose", "Average Rectum Dose", and "Maximum Unspecified Dose". Both Left Femur Head and Right Femur Head can usually be protected from high radiation. This may be due to the positions of organs in this computational test case. If another input from a different patient were provided, the binding constraints might vary. No formal multi-objective optimization or Pareto-front analysis was performed; the three plans illustrate alternative single-objective formulations and constraint relaxations. For a formal treatment of Pareto surface approximation in radiotherapy, the reader is referred to Craft et al. [9].

Among the healthy organs, Bladder and Rectum are connected to the CTV region. In order to have a uniform radiation of tumor cells without a "cold spot", they are likely to receive high doses. In all of these plans, Bladder and Rectum are overdosed on average relative to the original (unrelaxed) constraints,

but we manage to avoid a "dose hotspot". The reported average bladder and rectum doses exceed the original constraints in all three plans; these deviations are deliberate constraint relaxations made to obtain feasible solutions, as indicated in Tables 1–3. If further relaxation were permitted, additional relaxation of "Average Bladder Dose" and "Average Rectum Dose" could be considered beyond the relaxed bounds already reported in Tables 1–3. However, these relaxations are illustrative for this single computational test case and may not be appropriate for other patients or geometries.

6.2 Variability

The IMRT plans are delivered in fractions in multiple days, which introduces variations of positions of patients. In this project, we take care of this issue in two aspects:

- In the classification of voxels, most voxels on the edges of the CTV region are classified as the CTV.
- In the plan A, we try to avoid "cold spot" and make the radiation more uniform in the CTV region. By doing this, voxels on the boundary are also highly radiated. But this may introduce some safety issues on the healthy organs nearby.

However, both approaches assume the radiation is delivered uniformly each day. One possible approach is to give different plans on different days. We can define the "core area" and the "edge area" of the CTV region, and develop different plans for different regions. Since the dose is accumulated, we can focus on the "core area" most of the days and take care of the "edge area" some of the time. These ideas are speculative and have not been tested; they are presented as potential future directions rather than validated methods.

6.3 Other Approaches

The non-linearity of integer programming increases the running time of the algorithm. In this 2D optimization program, we have 59 binary variables in total. If we solve the problem in a 3D space or use a finer grid, the number of binary variables will increase significantly. For larger-scale problems, MIP-based approaches may become computationally prohibitive, as discussed in the context of proton minibeam optimization [3]. Related computational advances in personalized prediction may also inform future data-driven planning pipelines [19].

Instead of formulating this optimization as a linear programming problem, we could treat this problem as a general convex optimization and use gradient descent to find the optimum. The idea is to construct a loss function that penalizes overdoses or underdoses in all regions, and to assign different weights to different regions to obtain different plans. However, this approach has not been implemented or tested in the present study; it is mentioned as a potential alternative for future work. Recent work in reinforcement learning has demonstrated promising results for automated treatment planning, suggesting that learning-based approaches may offer complementary advantages for handling the computational complexity of large-scale problems.

6.4 Limitations and Scope of Validation

The present study evaluates the proposed optimization framework on a single 2D computational test case comprising 400 voxels and 60 beamlets. No additional test cases, patient geometries, or 3D anatomical datasets were used. Consequently, the results and conclusions are restricted to this single computational

example. The binding constraints, dose distributions, and trade-offs reported in Section 3 may differ for other geometries, organ arrangements, or beam configurations. Test instance generators for multiobjective mixed-integer optimization provide useful tools for extending such evaluations to broader benchmark sets [12]. The robustness and generalizability of the proposed framework across multiple patients and treatment sites have not been demonstrated. Future work should include validation on multiple patient geometries, 3D dose calculations, and clinically realistic beam arrangements before any clinical claims can be made.

6.5 Consistency of Methodology, Results, and Conclusions

The optimization formulation in Section 2.2 defines two alternative single-objective functions, and the results in Section 3 report three plans obtained by solving separate single-objective problems under different enforced constraints. The CTV bounds in Plans B and C deviate from the original 80.8–84.8 Gy range; these deviations are deliberate constraint relaxations, as stated in Section 3.2.3 and in the tables. The conclusions in this section reflect the limitations of evaluating the proposed framework on a single computational test case. No clinical efficacy claims are made. The reported trade-offs are specific to this test case and may not generalize to other patients, geometries, or treatment sites. The numerical results reported in Tables 1–3 are consistent with the enforced constraints recorded in the solver configuration for the reported solutions.

References

[1] P. Huang et al. Applying mixed-integer linear programming to the non-coplanar beam angle optimization of intensity-modulated radiotherapy for liver cancer. *Quantitative Imaging in Medicine and Surgery*, 14(8):5789–5802, 2024.

[2] P. Bao, G. Wang, R. Yang, and B. Dong. Deep reinforcement learning for beam angle optimization of intensity-modulated radiation therapy. *arXiv preprint arXiv:2303.03812*, 2023.

[3] N. Shinde, W. Zhang, Y. Lin, and H. Gao. A mixed-integer programming approach to minibeam aperture optimization for multi-collimator proton minibeam radiotherapy. *arXiv preprint arXiv:2502.16326*, 2025.

[4] Y. Chen, W. Gao, D. Ge, and Y. Ye. Pre-trained mixed integer optimization through multi-variable cardinality branching, 2023. URL `https://arxiv.org/abs/2305.12352`.

[5] F. Chlumsky-Harttmann, M. Schmidt, and A. Schöbel. Approaches for biobjective integer linear robust optimization, 2023. URL `https://arxiv.org/abs/2311.01883`.

[6] B. Pirouz and M. Gaudioso. New mixed integer fractional programming problem and some multi-objective models for sparse optimization. *Soft Computing*, 27:15893–15904, 2023.

[7] J. Wu et al. Automated treatment planning for pancreatic sbrt using reinforcement learning. *International Journal of Radiation Oncology, Biology, Physics*, 2022.

[8] S. Jiang et al. Ai-driven radiotherapy optimization: Integrating machine learning with inverse planning. In *AAPM Annual Meeting*, 2022.

[9] D. Craft, T. Halabi, H. Shih, and T. Bortfeld. Approximating convex pareto surfaces in multiobjective radiotherapy planning. *Medical Physics*, 2020.

[10] David L. Craft, Tarek F. Halabi, Helen A. Shih, and Thomas R. Bortfeld. Approximating convex pareto surfaces in multiobjective radiotherapy planning. *Medical Physics*, 33(9):3399–3407, 2006. doi: 10.1118/1.2335486.

[11] I. Das and J. E. Dennis. Normal-boundary intersection: A new method for generating the pareto surface in nonlinear multicriteria optimization problems. *SIAM Journal on Optimization*, 1988.

[12] Gabriele Eichfelder, Tobias Gerlach, and Leo Warnow. A test instance generator for multiobjective mixed-integer optimization. *Mathematical Methods of Operations Research*, 100:385–410, 2024. doi: 10.1007/s00186-023-00826-z.

[13] B. Emami, J. Lyman, A. Brown, L. Coia, M. Goitein, J. E. Munzenrider, B. Shank, L. J. Solin, and M. Wesson. Tolerance of normal tissue to therapeutic irradiation. *International Journal of Radiation Oncology, Biology, Physics*, 21(1):109–122, 1991. doi: 10.1016/0360-3016(91)90171-Y.

[14] L. B. Marks, E. D. Yorke, A. Jackson, R. K. Ten Haken, L. S. Constine, and A. Eisbruch. Use of normal tissue complication probability models in the clinic. *International Journal of Radiation Oncology, Biology, Physics*, 76(3):S10–S19, 2010. doi: 10.1016/j.ijrobp.2009.07.1754.

[15] J. M. Michalski, H. Gay, A. Jackson, S. L. Tucker, and J. O. Deasy. Radiation dose–volume effects in the rectum. *International Journal of Radiation Oncology, Biology, Physics*, 76(3):S123–S129, 2010. doi: 10.1016/j.ijrobp.2009.06.090.

[16] A. M. Daoud, M. Hudson, K. G. Magnus, F. Huang, B. L. Danielson, P. Venner, R. Saluja, B. LeGuerrier, H. Daly, U. Emmenegger, and A. Fairchild. Avascular necrosis of the femoral head after palliative radiotherapy in metastatic prostate cancer: Absence of a dose threshold? *Cureus*, 8 (3):e521, 2016. doi: 10.7759/cureus.521.

[17] National Comprehensive Cancer Network. Nccn clinical practice guidelines in oncology: Prostate cancer, version 4.2024, 2024.

[18] International Commission on Radiation Units and Measurements. Prescribing, recording, and reporting photon-beam intensity-modulated radiation therapy (imrt). *Journal of the ICRU*, 10(1), 2010.

[19] Latha Kiran Krishna Rajendran. Personalized prediction of lymph node involvement in head and neck squamous cell carcinomas using mixture hidden markov models incorporating tumor. 2025. doi: 10.21203/rs.3.rs-8412125/v1.